ORIGINAL ARTICLE

Composites of resorcinol and hexamethylenetetramine modified nanocellulose whiskers as potential biofiller in natural rubber latex: synthesis, characterization and property evaluation

Seena K. Thomas[1,2] · P. M. Sabura Begum[1] · P. Dileep[3] · K. V. Neenu[1] · Deepthi Anna David[1] · Ansa Santu[1] · C. D. Midhun Dominic[4]

Abstract

Surface modification of nanocellulose to improve its compatibility with the polymer matrix is gaining considerable attention these days. Herein, nanocellulose whiskers (NCW) extracted from *Acacia caesia* were modified with resorcinol and hexamethylenetetramine (RH) by the refluxing method. The characteristic properties of RH-modified NCW were studied using field emission scanning electron microscopy (FESEM), high-resolution transmission electron microscopy (HRTEM), energy dispersive X-ray spectroscopy (EDX), Fourier transform infrared spectroscopy (FTIR), dynamic light scattering (DLS), X-ray powder diffraction (XRD), thermogravimetric analysis (TGA) and UV–visible diffuse reflectance spectroscopy (UV-DRS). A marginal decrease in crystallinity index was observed by surface modification, whereas the thermal stability (T_{max}) of the NCW increases by 32 °C on surface modification. The potential of modified filler in improving the properties of natural rubber latex (NR) was studied by comparing its mechanical, thermal, diffusion, permeability and biodegradability properties with neat NR and NR-NCW composites. Upon 2 phr filler loading, the tensile and tear strengths of modified NCW composites increased by 26 and 38% accordingly compared to the NR-neat. The better filler matrix interaction resulted in the marginal positive shift in the glass transition temperature, transport properties and T_{max} of the modified composite. The incorporation of NCW also enhanced biodegradability and reduced the permeability of the prepared composites.

Keywords *Acacia caesia* · Hexamethylenetetramine · Nanocellulose whiskers · Natural rubber · Resorcinol

✉ Seena K. Thomas
seenamotty5@gmail.com

✉ C. D. Midhun Dominic
midhundominic@shcollege.ac.in

1 Department of Applied Chemistry, Cochin University of Science and Technology, Kerala 682022, India

2 Post Graduate & Research Department of Chemistry, Sree Sankara College, Kalady, Kalady P.O., Ernakulam Dist., Kerala 683574, India

3 J. J. Murphy Research Centre, Rubber Park India Pvt. Ltd., Airapuram, Kerala 683556, India

4 Department of Chemistry, Sacred Heart College (Autonomous), Thevara, Kochi, Kerala 682013, India

1 Introduction

Modern research is focused on biomaterial-based systems for producing fresh, eco-friendly and defensible goods due to environmental concerns and sustainability considerations [1]. To reduce the ecological problem, a biopolymer used in the elastomeric industry is natural rubber due to its high extensibility and use as a potential raw material in flexible packaging, gloves, food wraps, belts, foot wears, etc. However, the lower mechanical strength and abrasion resistance of the raw form of natural rubber limit its usefulness in diverse applications [2]. So, an effective filler should be provided to enhance the properties of natural rubber for forward looking requisites.

Lately, natural fillers like cellulose, lignin, starch, chitin, chitosan, xylose, etc. gained prominence in composite materials due to their environmental friendliness. These fillers can effectively minimize the drawbacks of petroleum based

fillers such as non-renewable origin, toxicity, pollution, high cost, etc. [3]. Nanocellulose is a biopolymer with high aspect ratio, surface area, mechanical and physicochemical properties, and hence it is a promising substitute for synthetic polymers derived from petrochemical sources [4]. According to current research, nanocellulose plays a prominent role in constructing high-performance natural rubber materials for advanced applications due to their superior features. It is considered a green filler for strengthening polymers because of its potential for fabricating value-added products without harming the surroundings [5]. The potential of cellulosic nanofillers in high-performance rubber bio-nanocomposites is constrained by agglomeration, although they represent a sustainable alternative to synthetic fillers [6]. Over the past decades, much effort has been given for incorporating nanocellulose in natural rubber to improve its characteristic properties [7]. A small amount of nanomaterial can enhance the composite properties to several orders of magnitude, and it is the prime cause to choose it as fillers. Enhancing the biodegradable property of the composite and reducing the abrasion resistance are some additional advantages of employing cellulose as filler in natural rubber [8]. But, the hydrogen bonds formed between the hydroxyl groups of β-1,4-D-glucopyranose units present in nanocellulose lead to easy agglomeration and make it difficult to be dispersed in matrices [9]. Moreover, the polar nature of nanocellulose and the nonpolar nature of natural rubber lead to poor interface interaction [5]. Nanocellulose can improve the physico-mechanical properties of the rubber composites at very low concentrations, but at higher concentrations, it can have negative impact on the properties due to the poor dispersion in the matrix, according to Singh et al. [10]. Jinitha et al. compared the reinforcing efficiency of unmodified and modified lignocellulosic wastes (sago seeds) with 37% cellulose content in styrene butadiene rubber (SBR) composites [11]. The study found that the modified sago seed/SBR composites had increased tensile and tear strength of 60 and 22% respectively, in comparison to the unmodified one. Consequently, the surface modification or chemical grafting of nanocellulose was found to be better preferences to solve this drawback [7].

By incorporating hydrophobic nature on nanocellulose, better compatibility with the hydrophobic matrix can be achieved and thereby properties of the biocomposites can be enhanced [1]. It is imperative to introduce either a charged or a hydrophobic moiety via surface modification to the composite in order to overcome the self-aggregation of the cellulose molecules within the hydrophobic matrix due to intra and inter molecular hydrogen bonding [3]. The surface modification of the nanocellulose includes acetylation, TEMPO oxidation, silylation, sulfonation, phosphorylation, amidation, carbamation, etc. using various surface modifiers or reagents [3]. By surface modification, the reduced

polarity of the nanocellulose roots the improved filler dispersion and enhance the compatibility between the hydrophobic matrix and the hydrophilic filler [10]. Jiang et al. recently developed natural rubber composites by partially replacing carbon black (CB) with cationic surfactant (cetyltrimethyl ammonium bromide (CTMAB)) modified nanocellulose (NCC) [12]. The study showed that the dispersion of the NCC was positively influenced by the surface modification and the tensile, tear and the elongation properties of the modified composites were increased by 7.2, 47.9 and 15% respectively. Cellulose nanofibers grafted with either –SH or –C=C functional groups was used by Sinclair et al. for developing SBR composites [13]. The surface functionalised nanofibers upon esterification reaction could readily increase the compatibility of the filler within the matrix and enhances its chemical linkages with the matrix. Subsequently, the modified cellulose nanofiber composites showed enhanced strength and modulus compared to the composite with same CB loading. Bis-(triethoxysilyl-propyl) tetrasulfide (TESPT) was utilized by Somseemee et al. for the surface modification of cellulose nanofibers for natural rubber (NR) composites [14]. The increased crosslink density in the presence of TESPT improved the modulus, tensile strength and hardness of the composites. The mixture of resorcinol and hexamethylenetetramine can be used with nanocellulose to reduce its hydrophilicity by forming hydrogen bonds between them. Hence, this can improve the interfacial adhesion between the rubber and the cellulose [9]. Partial replacement of silica in NR composites using cellulose nanocrystals (NCC) modified with resorcinol and hexamethylenetetramine was presented by Xu et al. [15]. The composite with 50% silica replaced with modified NCC showed an increase in tensile strength, tear strength and hardness of 10.5%, 29% and 19.5% accordingly with respect to the unmodified NCC composite. A similar study conducted by Jiang et al. also reported enhanced properties for the cellulose nanocrystals modified with resorcinol and hexamethylenetetramine [9].

The cellulose molecules has high propensity to aggregate due to the possibility of forming hydrogen bonds between the abundant hydroxyl groups. In order to make it more compactable with the natural rubber, the surface modification of the cellulose is necessary. The property of composites can be also tailored with surface modification. So the hypothesis of our work can be quoted as "is it possible to develop sustainable natural rubber composites using resorcinol and hexamethylenetetramine surface modified nanocellulose for high end applications". According to the author's knowledge, no work has been reported on the surface modification of nanocellulose whiskers using resorcinol and hexamethylenetetramine using refluxing method. So, the study preferably aimed at the synthesis and characterization of the nanocellulose and surface-modified nanocellulose and the properties its ability in uplifting the physico-mechanical

properties of the matrix while they are introduced to the natural rubber. Surface modification can enhance the nanocellulose whisker's interfacial adhesion and dispersion in the matrix. Consequently, the unique composite that the study offers will be a future promising material in the rubber sectors. The concept of using an end matter as worthy green filler for reinforcing a bio matrix always fulfils the need of sustainability in composite materials.

2 Materials and methods

2.1 Materials

Njavallil latex, Eloor, Kerala, India, supplied the centrifuged NR latex (Para rubber tree (*Hevea brasiliensis*), with a 60% dry rubber content, a 0.70% ammonia content and a 0.95 specific gravity). A plant bark of *Acacia caesia* fibres, an agro-waste collected from Ayurvedic hospitals in Ernakulum, Kerala, India, Resorcinol and hexamethylenetetramine (RH) was purchased from Amruta Industries, Mumbai, India. Dispersions of zinc diethyl carbamate (ZDC), sulphur (S), zinc oxide (zno), potassium oleate, vulcastab were purchased from Associate chemicals, Kochi, Kerala, India; Potassium hydroxide (KOH) and toluene were kindly supplied by Merck, Bombay, India.

2.2 Methods

2.2.1 Modification of NCW with Resorcinol formaldehyde by refluxing

The sulphuric acid hydrolysis was used to create nanocellulose whiskers from *Acacia caesia* fibres ('Incha') with a size range of 30 nm. The detailed method for the extraction of NCW is discussed in our previously reported work [16]. Resorcinol (1.56 g) and hexamethylenetetramine (1 g) (RH) were mixed well in a mortar. It was then added to nanocellulose whiskers (NCW) dispersion and the mixture was refluxed in two neck RB flask under magnetic stirring at 55–60 °C for 5 h. The mixture was cooled, filtered and washed with water until the filtrate became a colourless solution. It was then dried in an air oven at 50 °C for analysis.

2.2.2 Latex compounding and film casting

The latex compounding technique was used to prepare NR gum and NR-NCW-RH nanocomposites according to the formulation given in Table 1. The nanocomposites with 0, 1, 2, 3 and 4phr (parts per hundred rubber) NCW-RH were prepared by adding water dispersion of nanocellulose in NR latex. This mixture was stirred for 30 min, followed by other ingredients in the formulation as dispersion, and

Table 1 Formulation of NR-NCW-RH composites

Materials	Amount (g)
60 % DRC in centrifuged NR latex	167.0
NCW-RH	As per requirement
10% Potassium hydroxide solution	1.0
10% Potassium oleate solution	1.0
20% Vulcastab VL	1.0
50% Zinc oxide dispersion	1.0
50% ZDC dispersion	2.0
50% Sulphur dispersion	3.0

then ultrasonicated. The NR gum and NR NCW-RH mixtures were cast into a glass tray and kept overnight at room temperature. Vulcanized films were prepared after drying and curing in a hot air oven at 50 °C for 24 h and then at 100 °C for 45 min. Before starting the characterization, these cured films were placed at 30 °C temperature and 50% humidity for **1** day.

The scheme of plausible reaction is given in Fig. 1. Hydrogen bonds formed between the hydroxyl groups are shown here. The hexamethylenetetramine on hydrolysis gives formaldehyde and ammonia molecules [17]. The number of free hydroxyl groups in cellulose decreases by the modification process, making it less hydrophilic and thus more hydrophobic. While considering the reactivity of resorcinol, the hydrogen atoms of carbon adjacent to the hydroxyl groups such as C_2, C_4 and C_6 are reactive. However, the hydrogen atom at C_5 is primarily unreactive. Hexamethylenetetramine produces activated methylenes while curing, which react with resorcinol forming resorcinol formaldehyde resin [18]. In this reaction between resorcinol and hexamethylenetetramine, the former acts as a methylene acceptor and the latter as a methylene donor. Thus methylene crosslinks are formed between resorcinol molecules [19]. Cellulose forms hydrogen bonds with these cross-linked resorcinol molecules to get a uniform dispersion. The hexamethylenetetramine acts as a methylene donor and thus forms a cross-linked structure between resorcinol molecules. The hydroxyl groups present in the complex form hydrogen bonds with NCW. This modified NCW-RH forms a chroman ring with an isoprene unit, schematically represented in Fig. 2.

2.3 Characterizations

2.3.1 Morphological studies

The morphology of samples was analysed using Hitachi SU6600 variable pressure field emission scanning electron microscope (FESEM) at an acceleration voltage of 30 kV and Probe current of 1 pA–200 nA. Samples were sputter-coated with gold to avoid charging. The transmission

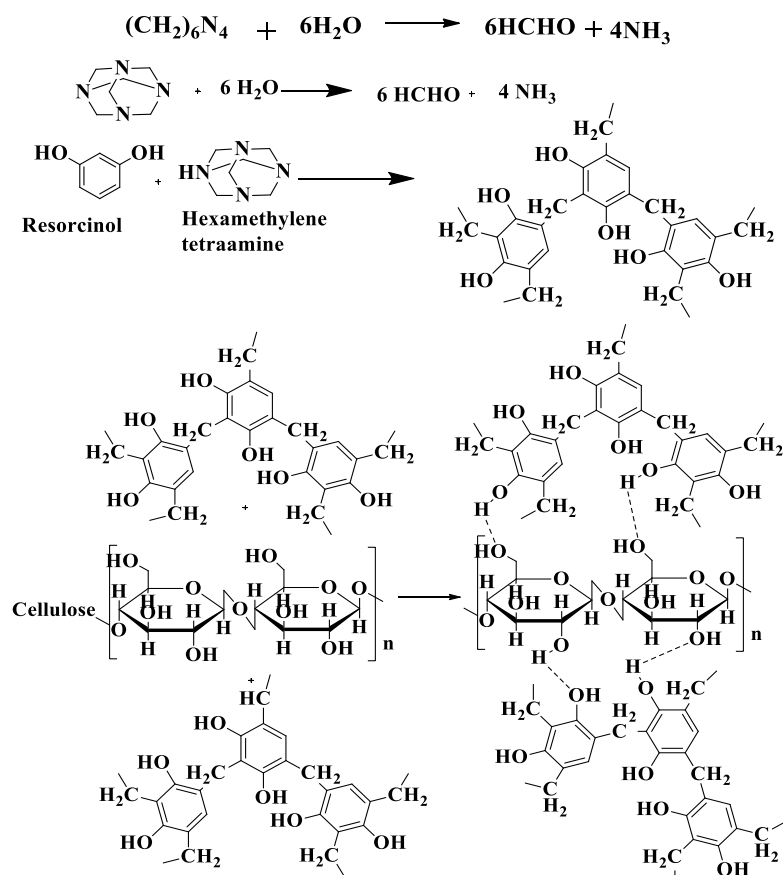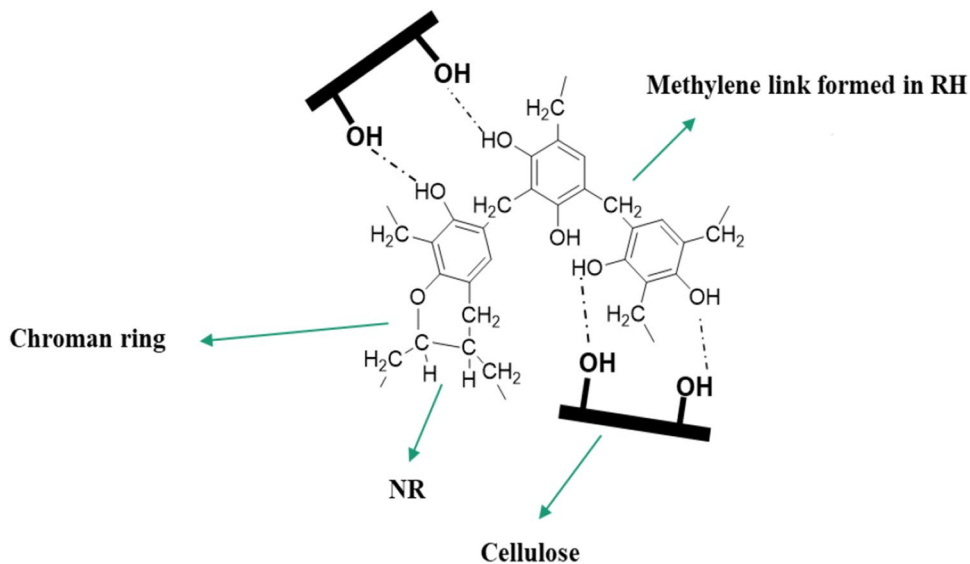**Fig. 1** Schematic representation of plausible reaction of NCW with RH

Fig. 2 Scheme of plausible reaction of composite formation [20]

electron micrographs of dilute dispersion of cellulose nanofibres were obtained on a high-resolution transmission electron microscope, JEM-2100 HRTEM. A drop of suspension of each sample was placed on a carbon film-coated copper grid, dried up and examined.

2.3.2 Elemental studies

The elemental composition of materials was obtained using Joel 6390LA/ OXFORD XMX N scanning electron microscopy with energy dispersive X-ray spectroscope.

2.3.3 Structural analysis

The FTIR spectrum was recorded using Avtar 370 spectrometer (Thermo Nicolet, USA). The powdered samples were mixed well with potassium bromide (KBr) and pressed to form KBr thin pellets. The scanning was performed at the range of 4000 to 400 cm^{-1} at a resolution of 4 cm^{-1} with 32 scans per min. The average particle size distribution of the isolated cellulose nanofibres was carried out using Malvern zetasizer instrument (Malvern Instruments Ltd.). The suspension of NCW and NCW-RH were ultrasonicated before analysis. The measurements were conducted triplicated, and the average of the measurements was reported.

2.3.4 Absorbance studies

UV diffuse reflectance spectrometer using DH-2000-BAL deuterium-halogen light source was used for studying the UV absorbance of NCW-RH.

2.3.5 Crystallinity studies

The crystallinity of the samples was recorded on Bruker AXS D8 Advance with Cu Kα radiation with an angle range 5°–80° (2θ angle range) at a wavelength of 1.541 Å, an operating voltage of 45 kV and a current of 35 mA. The Segal equation was used to calculate the crystallinity index (*Ic*) of raw fibres and prepared NCW [21, 22] is given as,

$$I_c = \left[\left(I_{(200)} - I_{(am)} \right) / I_{(200)} \right] * 100 \tag{1}$$

*w*here $I_{(200)}$ is the peak intensity at $2\theta = 22.6°$ and $I_{(am)}$ is the intensity minimum between 200 and 110 plane ($I_{(am)}$, $2\theta = 16$).

2.3.6 Thermal studies

The thermal analysis is performed using a TGA Q50 (TA Instruments) heated at a rate of 20 °C/min in a nitrogen environment at temperatures ranging from 25 to 800 °C. Diffuse reflectance spectroscopy, or diffuse reflection spectroscopy, is a subset of absorption spectroscopy. Differential scanning calorimetry was performed using Netzsch DSC 204 F1 (Germany) at a heating rate of 10 °C/min in inert nitrogen atmosphere at a temperature range from −70 to 160 °C.

2.3.7 Mechanical analysis

The stress-strain measurements were conducted on Instron make Universal Testing Machine using dumbbell specimens by ASTM-D-412. Tensile strength, elongation at break and tensile modulus were recorded and calculated by the instrument software. The tear strength of composites was tested according to the ASTM D-624 standard. The tensile fracture surfaces of samples were studied using NOVA NANO FESEM 450 model. Attenuated total reflection Fourier transform infrared spectroscopy (ATR-FTIR) spectrum was recorded using Avtar 370 spectrometer (Thermo Nicolet, USA) in the ATR mode.

Dynamic mechanical analysis is used to identify the ability of a sample to store and diffuse mechanical energy when subjected to deformation in a wide temperature range which was studied using TA Instrument DMA Q800, in tension mode from −100 to 90 °C at a testing frequency of 1 Hz and heating rate of 3 °C/min.

2.3.8 Diffusion studies

The procedure of diffusion studies is as follows. The prepared samples were cut into 1 cm diameter and dried at 50 °C for 12 h, then measured the weight. Then all samples were immersed in toluene, and the solvent uptake was measured at different time intervals. Swelling index, mol percentage uptake and crosslink density of samples were measured by swelling the samples in toluene. The mole percentage solvent uptake (Qt %) was calculated by using the equation,

$$Qt\ mol\% = \frac{(W_t - W_i)/M_s}{W_i} \times 10 \tag{2}$$

where W_t is the weight of the swelled sample after time t and W_i is the initial weight of the sample before swelling, M_s is the molecular mass of solvent.

The following equation calculated the swelling index,

$$Swelling\ index = \frac{(W_s - W_i)}{W_i} \times 100 \tag{3}$$

where W_i implies the initial weight of sample before swelling and W_s is the maximum swollen weight.

For the calculation of crosslink density, the rubber solvent interaction parameter has been found using the equation,

$$\chi = \beta + \frac{V_s (\delta_s - \delta_p)^2}{RT} \tag{4}$$

where V_s is the molar volume of the solvent, δ_s and δ_p are solubility parameters of solvent and polymer. R is the universal gas constant and T the absolute temperature, β is the lattice constant and is 0.38 in this calculation.

Using χ values, the molar mass between crosslinks (M_C) of the polymer was estimated from the Flory-Rehner equation,

$$M_C = \frac{-\rho_p V_s \left(V_r\right)^{\frac{1}{3}}}{\ln\left(1 - V_r\right) + V_r + \chi V_r^2} \qquad (5)$$

where ρ_p is the density of the polymer, V_r is the volume fraction of swollen polymer, V_s is the molar volume of the solvent and χ the interaction parameter. The volume fraction of the polymer is calculated by the equation,

$$V_r = \frac{(d - fw)\rho_r^{-1}}{\left(d - f_w\right)\rho_p^{-1} + A_o\rho_s^{-1}} \qquad (6)$$

where d is the desorbed weight of the polymer, f is the weight percent of filler, w is the initial weight of the polymer, ρ_p and ρ_s are the density of polymer and the solvent, respectively and A_o is the net solvent uptake of the polymer. Using the M_c values, crosslink density can be calculated by the equation

$$\text{Crosslink density, } \upsilon = \frac{1}{2M_c} \qquad (7)$$

2.3.9 Biodegradation studies

The biodegradation of NR/cellulose whiskers nanocomposites in soil was carried out [23]. The soil was taken from the surface layer. To obtain a homogeneous mass, all the inert materials were removed. A thickness of 3 cm was obtained by pouring 100 g of soil into a plastic pot (30 cm × 15 cm). All the aforementioned compositions were accurately weighed, along with nanocomposite samples. The samples were previously dried at 50 °C for 24 h. After which, they were buried in the pots to a depth of 1 cm. As to sustain the moisture, water was sprayed once a day. The samples were buried for four weeks but were also weighed each week too. The samples were taken out carefully, washed with distilled water, dried at 50 °C for 24 h and then weighed, which was repeated after each period. To determine the average weight loss, the following equation can be used.

$$\text{Weight loss } \% = \frac{W_0 - W_t}{W_0} \times 100 \qquad (8)$$

Where W_0 is the initial weight and W_t is the remaining weight at any time. All results are the average of three replicates. The purpose of this study was to monitor the biodegradation of our test samples using the composting setup outlined in ASTM D 5338-15 [24].

2.3.10 Wettability studies

Water contact angle measurement is the most common method used to quantify the wettability of a solid surface by a liquid. The contact angle is geometrically defined as the angle formed by a liquid at the three phase boundary where a liquid, gas, and solid intersect.

2.3.11 Gas permeability studies

A Lyssy Manometric gas permeability tester L100-2402 was used to measure the air permeability of the NR-NCW composite membranes. The test gas selected was nitrogen, and it was used at a flow rate of 500 mL/min. The circular-shaped samples having a diameter of 1 mm were used. The equation used to calculate the permeability of the test samples is,

$$P_m = \left(T_r * P_r\right)/t_m \qquad (9)$$

where P_m is permeability of the test sample, t_m is interval time constant for the test sample, P_r is permeability of the reference (standard PET sample) and T_r is interval time constant for standard PET. The temperature and relative humidity conditions of the test are (25 ± 1) °C and (65 ± 0.5), respectively.

3 Results and discussion

3.1 Morphological analysis of modified filler

The FESEM of NCW and RH-modified NCW (NCW-RH) are shown in Fig. 3(a) and (b). A surface coating on the modified NCW is visible in this image which might have helped the NCW for avoiding self-agglomeration and thereby forms uniform dispersion of filler. Singh et al. also observed the reduced agglomeration of surface modified nanocellulose using 3-aminopropyltriethoxysilane [10]. The roughness of the cellulose whiskers increased after modification and each rods is covered by the resorcinol-hexamethylene complex through H-bonding. Figure 3(c) and (d) shows HRTEM images of NCW and NCW-RH. The strong hydrogen bonding between the NCW and RH hydroxyl groups aids in the absorption of RH particles on the NCW rods, allowing them to disperse uniformly and without agglomeration. This demonstrates that the surface modification was successful, as well as the high dispersion of the modified nanocrystals. A similar TEM images was presented by Souza et al. on surface-modifying nanocellulose with anionic surfactant by adopting ball milling method [25].

3.2 Energy dispersive X-ray spectrum

Energy dispersive X-ray spectroscopy (EDX) spectrum of NCW and NCW-RH are shown in Fig. 4. From this graph, a clear idea about the elemental analysis of the sample is

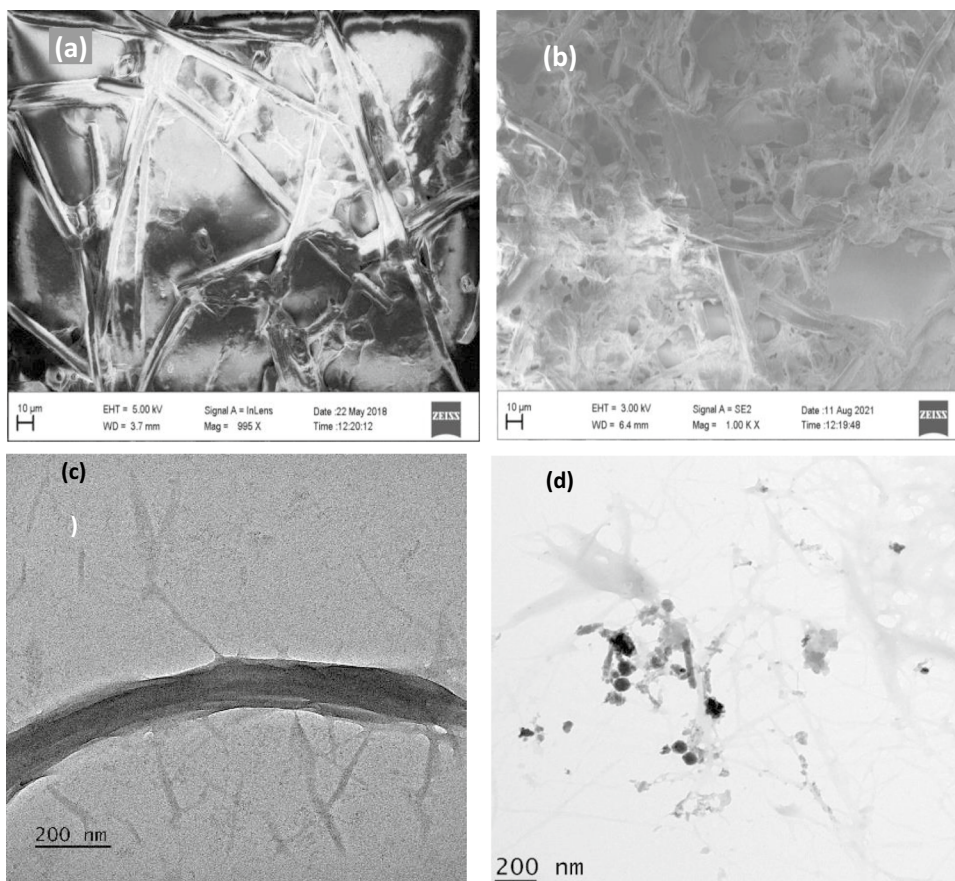**Fig. 3** FESEM micrographs of (**a**) NCW, (**b**) NCW-RH and TEM image of (**c**) NCW and (**d**) NCW-RH

Fig. 4 EDX Analysis of (**a**) NCW and (**b**) NCW-RH
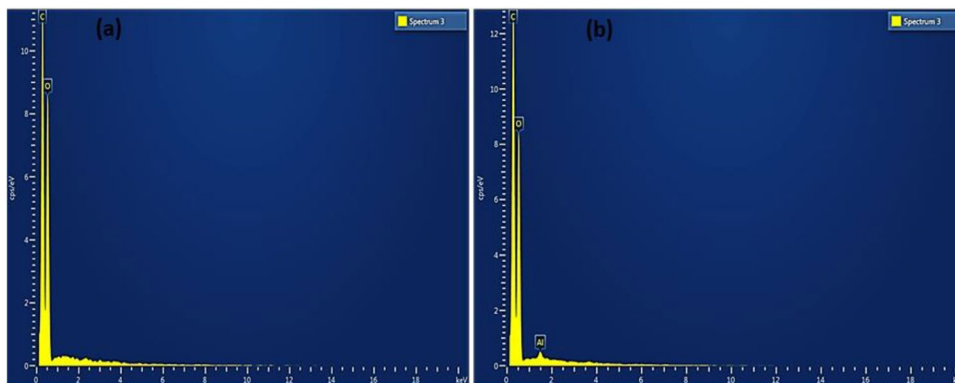
Table 2 Elemental analysis of NCW and NCW-RH

Sample	C (wt%)	O (wt%)
NCW	33.18	66.82
NCW-RH	37.69	62.15

3.3 Dynamic light scattering

The graphical representation of dynamic light scattering (DLS) is given in Fig. 5. The calculated average diameters for NCW and NCW-RH are 32.1 nm and 40.5 nm respectively. The diameter of the sample retained its nanometer range, even after its modification, which is an advantage for the composite reinforcement. Foo et al. reported a similar increase in the average diameter of the nanocrystalline cellulose modified with tannic acid and decylamine [26]. However, this slight increase in the diameter might

obtained. An increase in weight percentage of carbon and decrease in oxygen weight percentage indicate the successful incorporation of resorcinol formaldehyde in NCW. Table 2 tabulating the weight percentages of each sample also confirms the filler purity.

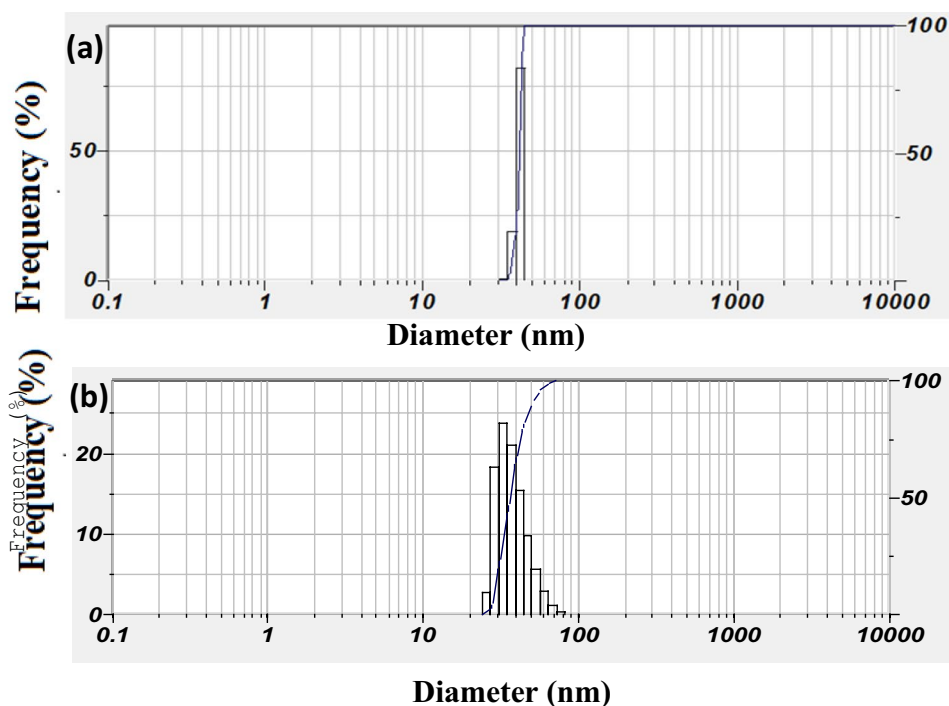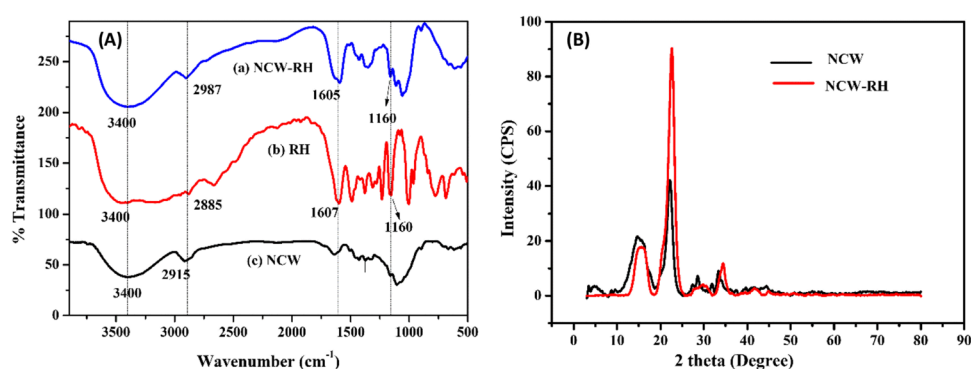**Fig. 5** Particle size distribution of (**a**) NCW and (**b**) NCW-RH

Fig. 6 (**A**) FTIR spectra of (a) NCW-RH (b) RH (c) NCW and (**B**) XRD pattern of NCW and NCW-RH

be an indication of the surface covering of NCW with RH complex.

3.4 Fourier transform infrared spectrum

The interaction between NCW and RH is proved in the FTIR spectrum given in Fig. 6(A). The absorption peaks at 3400 cm^{-1} in all samples indicate –OH's stretching vibration, and it is much more broadened for NCW-RH due to the formation of hydrogen bonds between NCW and RH [7]. -C-H symmetric stretching vibration is denoted by the absorption peak 2885 cm^{-1}. The peak at 1607 cm^{-1} shows the skeletal vibration of aromatic -C=C in RH, which is observed at 1605 cm^{-1} in NCW-RH also. The peak at 1160 cm^{-1} implies the –C=O stretching vibration [27].

3.5 X-ray powder diffraction

X-ray powder diffraction (XRD) patterns of NCW and NCW-RH are shown in Fig. 6(B). Almost same peaks are observed in both XRD diffractograms. The prominent peaks at 2θ = 16° and 22.6° correspond to (110) and (200) lattice planes of cellulose [16].The crystallinity index is calculated by Segal equation [22]. The crystallinity index of NCW is decreased from 79.65 to 77.84% after modification as given in Table 3. According to Somseemee et al., the reduction in

Table 3 Crystallinity index (I$_c$) of NCW and NCW-RH

Sample	Crystallinity index
NCW	79.65
NCW-RH	77.84

the number of hydrogen bonds in NCW leads to an unfavourable condition for crystallisation [14]. The crystallinity is also considered an essential factor in reinforcing a matrix while affecting its modulus. So it should be careful in selecting the surface modifier so as to retain the crystallinity even after the modification [5].

3.6 Thermo gravimetric analysis

The thermogravimetric analysis (TGA) and DTG images of NCW and NCW-RH are compared in Fig. 7(a) and (b). Dramatic increase in the onset degradation temperature from 252 to 296 °C is due to the modification with RH and is given in Table 4. The temperature at 50% degradation and maximum degradation temperature of NCW-RH also show a significant change after modification. This implies that there is an increase in thermal stability of the RH-modified NCW than the unmodified one.

3.7 UV–visible diffuse reflectance spectroscopy

Solid state UV–Vis diffuse reflectance spectrum of NCW-RH is plotted with Kubelka Munk model in Fig. 8. According to the literature, the absorption band observed for NCW is approximately near 279 nm [28]. This peak is reproduced in the modified NCW, indicating no change in the cellulose's essential characteristics on modification. The direct band gap (E_g) of the sample was estimated as 1.8 eV using the graph plotted with $(h\nu F(R))^2$ versus photon energy ($h\nu$), where F(R) is Kubelka-Munk function $[F(R)=(1-R)^2/2R]$ [29].

3.8 Morphological analysis of composites

The HRTEM image of the NR-NCW-RH-2phr composite is given in Fig. 9(A)(a) and (b9). The mechanism involved in latex film formation is summarised here. Evaporation of water during film formation restricted the Brownian motion of latex particles so that the water-air interfacial tension helped to form a continuous film. Curing makes it more homogeneous due to gradual coalescence by polymer chains'

Table 4 Thermal degradation data

Sample	Onset degradation temperature T_{on} (°C)	Temperature at 50% degradation T_{50} (°C)	Maximum degradation temperature T_{max} (°C)
NCW	252	322	332
NCW-RH	296	355	364

inter diffusion that removes the particle boundaries [30, 31]. The composite is produced by mixing RH-modified NCW with natural rubber latex and the compounding ingredients. The process of curing pushed the nanoparticles of NCW-RH to the boundary of spherical rubber latex particles. The thick rubber latex prevents the penetration of NCW-RH into the rubber spheres. The segregated network throughout the composite in the present work is illustrated with the HRTEM image. Latex stage mixing method helps in the formation of segregated network and uniform distribution of NCW-RH in NR latex and thereby the former wraps the latter during the film formation to get an excellent segregated network. A similar observation was also reported by Neena et al. [30].

The tensile fracture surface morphology is presented in Fig. 9(B)(c) and (d). Usually, the fracture in rubber composites is either by breakage of filler or pull-outs of agglomerated fillers from the matrix. NR gum shows a smooth surface, whereas NR-NCW-RH-2phr has a rough morphology. The addition of filler creates a rough and irregular fracture topography to the composite [32]. The craters and wrinkles which are seen on the fractured surface of NR-NCW-RH-2phr implies the effective stress transfer between the matrix and filler leading to better mechanical properties due to the slow fracture process [33].

3.9 Mechanical properties

The mechanical properties of NR-NCW-RH nanocomposites with different compositions prepared by latex stage processing technique are given in Table 5. The effect of NCW-RH on NR is very significant in terms of the increase in tensile strength, tensile modulus and tear strength. A vital decrease in elongation at break is also observed as the filler loading

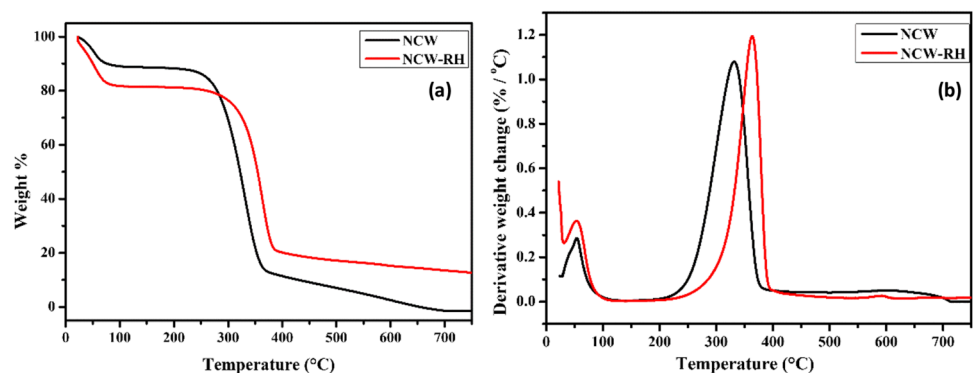**Fig. 7** (**a**) TGA and (**b**) DTG curves of NCW and modified NCW-RH
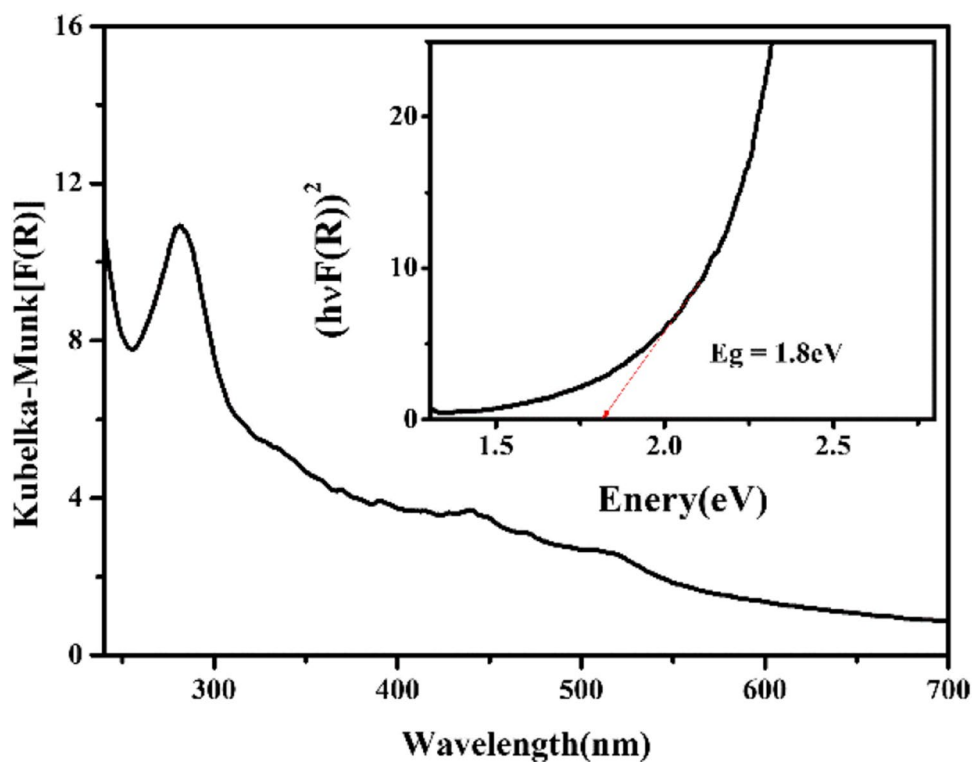
Fig. 8 UV-DRS spectrum of
NCW-RH

Fig. 9 (A) HRTEM image of
NR-NCW-RH-2phr in (**a**) 200
nm and (**b**) 50 nm, (B) FESEM
micrographs of (**c**) NR-gum and
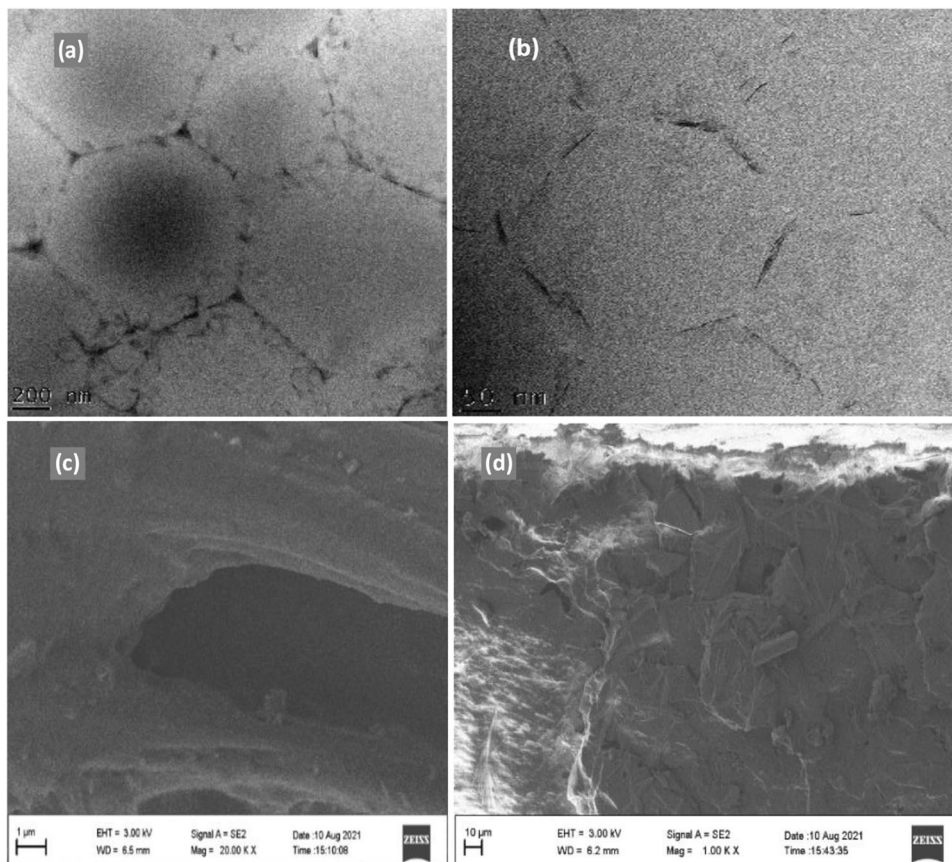(**d**) NR-NCW-RH-2phr tensile
fracture surfaces

Table 5 Mechanical properties of NR and NR-NCW-RH composites

Sample	Tensile strength (MPa)	Elongation at break (%)	Modulus at 500% elongation (MPa)	Tear strength (N/mm)
NR-gum	21.31 ± 0.60	1583 ± 43	1.14 ± 0.05	42.22 ± 1.3
NR-NCW-RH-1phr	24.23 ± 0.40	1556 ± 40	2.03 ± 0.07	47.53 ± 0.8
NR-NCW-RH-2phr	26.91 ± 0.60	1098 ± 56	3.09 ± 0.04	58.30 ± 1.0
NR--NCW-RH-3phr	26.18 ± 0.50	1079 ± 53	2.96 ± 0.03	49.98 ± 1.2
NR-NCW-RH-4phr	23.60 ± 0.30	1059 ± 48	3.57 ± 0.05	44.39 ± 1.3

increases. The tensile strength of NR has been improved by 26.3%, tensile modulus by 171.1% and tear strength by 38.1% by the addition of 2phr of NCW-RH. So, 2phr concentration for this particular filler in NR is considered as optimum for obtaining maximum properties. Its uniform distribution in NR is evident from the fracture SEM given in Fig. 9. The increased mechanical properties stem from a combination of two factors; first, the reinforcement in the network structure formed by the NCW-RH in the interfaces of rubber, which can transfer the load from matrix to filler, and second is the percolation effect of the filler in the rubber. The percolation effect occurs at a particular volume fraction threshold of filler in the matrix. A strong network is formed by reducing the distance between the particles in the composite [34]. However, beyond this concentration, the composite property decreases due to the altered crystalline structure. The mechanical properties are directly related to the degree of crystallinity. The less uniform distribution at higher filler loadings leads to a drop of film crystallinity and a decrease in tensile strength [32]. The stress-strain plot of NR gum and NR-NCW-RH with different compositions is given in Fig. 10(a). According to the literature, a strain-induced crystallisation is formed inside the rubber polyhedra without any interference from the filler particles. Eventually, the uniform distribution of filler and the strain-induced crystallisation are the two factors that prevent premature tearing at the interface which enhance the mechanical properties [30]. A decrease in elongation at break is observed as the filler loading increases, which in turn causes a reduction in elasticity for the NR-NCW-RH composite. The

three-dimensional network formed in the composite by the NCW-RH filler restricts the mobility of NR chains which in turn reduces its elasticity [32].

3.10 Attenuated total reflection Fourier transform infrared spectroscopy

Figure 10(b) represents the attenuated total reflection Fourier transform infrared spectroscopy (ATR-FTIR) of NCW-RH, NR gum, and NR-NCW-RH composites of different filler loadings. Some of the characteristic absorption bands of NR gum are -C-C stretching, -CH$_3$ bending and –CH$_2$ bending, which are denoted by the peaks such as 1013, 1377 and 1442 cm^{-1}, respectively [35]. The peak at 1667 cm^{-1} indicates the stretching vibration of C=C of the polyisoprene unit. Three nearby sharp peaks at 2850, 2931 and 2965 cm^{-1} imply –CH$_2$ symmetric stretching, –CH$_2$ asymmetric stretching and –CH$_3$ asymmetric stretching respectively. The broad peaks observed in composites between 3100 and 3600 cm^{-1} indicate the hydrogen bonds formed during composite preparation due to hydroxyl groups in cellulose [32].

3.11 Dynamic mechanical analysis

Dynamic mechanical analysis (DMA) is used to understand the ability of a material to store and dissipate mechanical energy when subjected to deformation by varying temperatures. The viscoelastic and damping characteristics of composites can be calculated by this analysis. The interaction between filler and matrix is also investigated. Figure 11

Fig. 10 (**a**) Stress-strain plot. (**b**) ATR-FTIR spectra of NR-gum and NR-NCW-RH composites
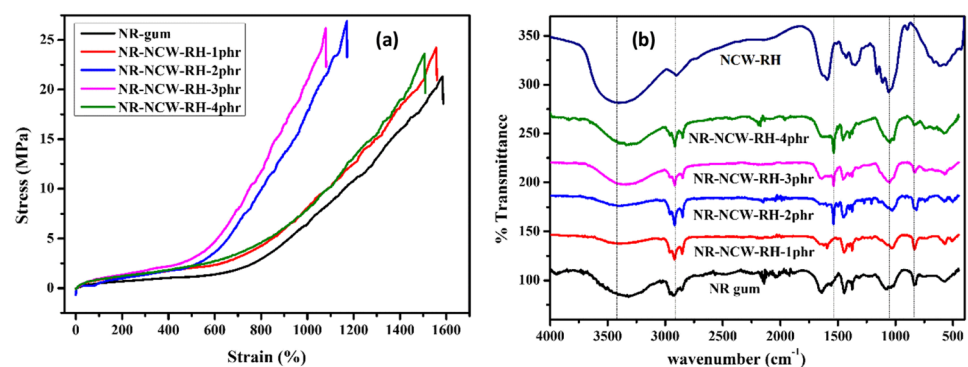
shows the variation of storage modulus (E′), loss modulus (E″) and tan δ with temperature and the respective values are summarised in Table 6. A Cole-Cole plot is also included here. The storage modulus decreases with temperature through three regions: glassy state in low temperature, a rubbery state in high temperature and the transition state from glassy to rubbery state, representing the glass transition temperature (T_g). Here, it is found that NR-NCW-RH-2phr composite has higher storage modulus than NR-NCW-2phr indicating the homogeneous dispersion of NCW-RH in the NR matrix. It is also directly related to the composite's crosslink density and is supported by the data given in Table 8. The storage modulus at 25 °C of NR-NCW-2phr and NR-NCW-RH-2phr composites are 1.631 and 2.539 MPa, respectively, representing the high crystallinity of the modified composite compared to the unmodified composite [32].

The energy lost during friction in composites is represented by loss modulus. The glass transition temperature, T_g, from the loss modulus curve for NR-NCW-2phr and NR-NCW-RH-2phr are −56.3 and −56.17 °C respectively. There is a marginal positive shift in the T_g for modified composites indicated its better filler-matrix interaction. The ratio of loss modulus and storage modulus is the damping factor (tan δ). The peak height from the graph of tan δ is also used to determine the glass transition temperature. However, there is no significant change in T_g for NR-NCW-RH-2phr and NR-NCW-2phr. The decrease in the intensity of the peak of the tan δ curve implies the restriction of the segmental movement of polymer chains in the NR-NCW-RH-2phr composite

Table 6 Dynamic mechanical analysis data of NR-NCW-2phr and NR-NCW-RH-2phr composite

Properties	NR-NCW-2phr	NR-NCW-RH-2phr
T_g (according to tanδ max) (°C)	− 48.22	− 48.37
T_g (according to E" max) (°C)	− 56.3	− 56.17
Tan δ at 25 °C	0.0438	0.1098
Storage modulus at 25 °C (MPa)	1.631	2.539
Volume fraction of immobilised polymer chain, C_v	0.0045	0.0208
Adhesion factor, A	0.0162	− 0.1309

compared to the unmodified one. It might be due to the stiffness produced by the NCW-RH filler in the NR matrix due to the better interfacial reinforcement in the composite [36].

The Cole-Cole plot or Wicket plot is drawn by the data of loss modulus against storage modulus. It is used to study the degree of homogeneity in the composite and to identify the structural changes by adding filler [37]. The smooth semicircular arc represents homogeneous polymer systems, and the irregular shape implies its inhomogeneity due to the phase separation [38, 39]. The Cole-Cole plot of the NR-NCW-2phr and NR-NCW-RH-2phr are shown in Fig. 11d. A smooth semicircular arc is obtained for the composites denoting the homogeneous nature of composites without any phase separation. From Table 6, the value of volume fraction of immobilised polymer chain (C_v) for NR-NCW-RH-2phr is 0.0208, which is

Fig. 11 DMA plots (**a**) storage modulus, (**b**) loss modulus, (**c**) tan delta curves and (**d**) Cole-Cole plot of NR NCW-2phr and NR−NCW-RH-2phr nanocomposites
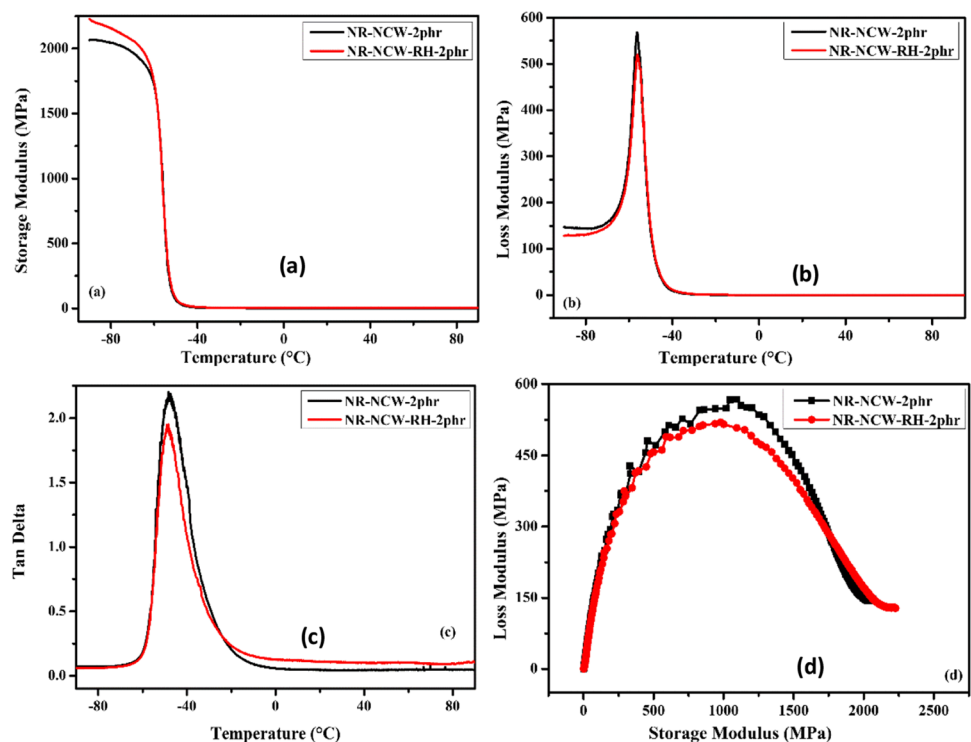
higher than 0.0045 of NR-NCW-2phr, indicating better interfacial interaction of filler and polymer chain in modified composite. Similarly, the adhesion factor of modified sample is less than the unmodified one, which is also a positive symbol of good interfacial interaction. As the adhesion factor decreases, the adhesion between the matrix and filler increases [40].

3.12 Thermal properties

By thermogravimetric analysis, the reduction in the weight percentage of sample material is measured at 0 to 800 °C in a nitrogen atmosphere. It is graphically plotted in Fig. 12. Due to the degradation of polymer part by chain scission or crosslink breakage, a sudden loss of weight appeared near 300 °C [41]. Thermal degradation data is given in Table 7. The onset degradation temperature of NR-NCW-RH-2phr is 7 °C greater than NR-NCW-2phr, T_{50} is 5 °C greater than NR-NCW-2phr and the maximum degradation temperature is 2 °C greater than unmodified cellulose composite. This implies a significant increase in thermal stability of the modified composite compared to the unmodified one.

3.13 Differential scanning calorimetry

The graphical representation of the differential scanning calorimetry (DSC) plot of NR gum, NR-NCW-2phr, and NR-NCW-RH-2phr is shown in Fig. 12(C). The glass transition temperatures, T_g, obtained from the graph, − 59.2, − 60.7, and − 59.8 °C respectively for the abovementioned samples does not have any significant change regardless of the nature of the filler. It might be due to retaining the chemical structure of natural rubber without forming any covalent bonds other than hydrogen bonding between natural rubber and the additives during compounding [42, 43].

3.14 Diffusion studies

The toluene uptake of NR-gum and NR-NCW-RH composites in varying NCW-RH loadings at different time intervals are shown in Fig. 13(a). The initial rate of solvent uptake is very high due to the high concentration gradient of the penetrant in the composite. Eventually, the concentration gradient reduces, and so the rate of solvent uptake also reduces.

Fig. 12 (**a**) TG, (**b**) DTG graphs and (**c**) DSC graphs of NR-gum, NR-NCW 2phr, NR-NCW-RH-2phr composites
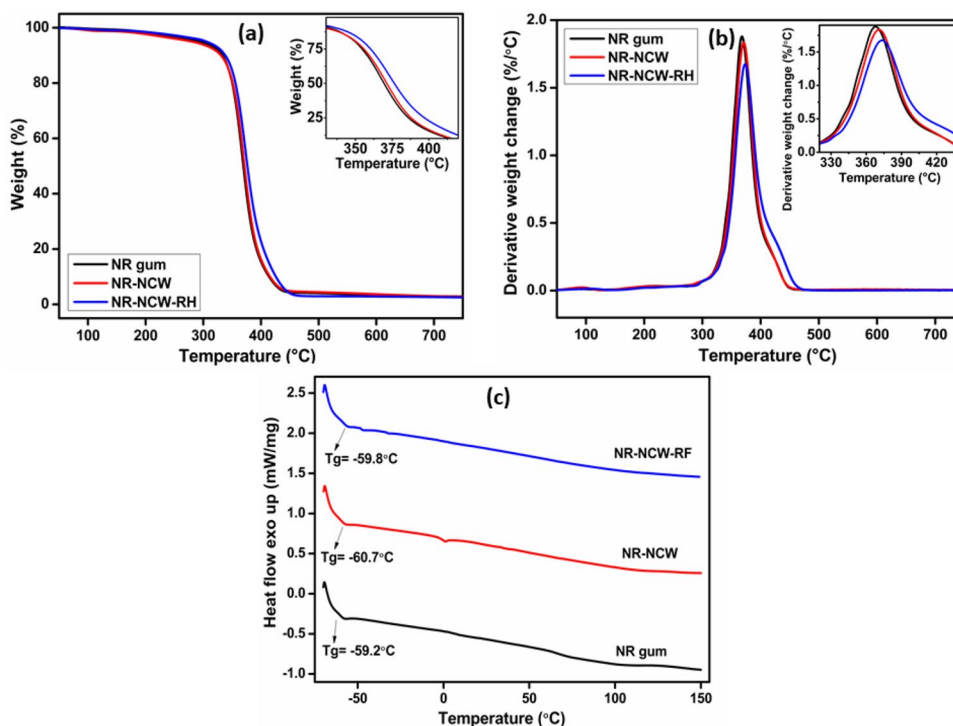

Table 7 Thermal degradation data of the composites

Sample	Onset degradation temperature T_{on} (°C)	Temperature at 50% degradation T_{50} (°C)	Maximum degradation temperature T_{max} (°C)
NR gum	333	370	368
NR-NCW-2phr	331	371	371
NR-NCW-RH-2phr	338	376	373

The chemical crosslinks and elastomer-filler interaction influenced the crosslink density of nanocomposites [44]. Table 8 shows the crosslink density and swelling index of all composites. NR-NCW-RH composites exhibited a reduction in solvent uptake with NCW-RH concentration. Higher crosslink density and lower swelling index were obtained for NR-NCW-RH-2phr composite, representing improved rubber-filler interactions. The crosslink density of the composite about 45% higher than the NR gum implies the superior interaction between the filler and matrix. The uniformly distributed NCW particles restrict the polymer chain's mobility, reducing the solvent uptake [45, 46].

3.15 Contact angle of water

The difference in hydrophilicity of the NR-NCW-RH-2phr composite compared to the NR-NCW-2phr composite is identified by the contact angle of water analysis. Hydrophilicity is directly proportional to the number of hydroxyl groups present in the composite. NCW is hydrophilic due to the presence of hydroxyl groups. However, NR is hydrophobic. Nevertheless, modifying NCW with resorcinol hexamethylene complex decreases the number of free hydroxyl groups due to the hydrogen bonding between cellulose and RH. The water contact angle for hydrophilic substances is smaller than that of hydrophobic substances.

**Table 8** Transport properties of NR-gum and NR-NCW-RH composites

Sample	Crosslink density (10^{-5} mol/g)	Swelling index (%)
NR-gum	4.9 ± 0.05	525 ± 5
NR-NCW-RH-1phr	6.1 ± 0.1	466 ± 3
NR-NCW-RH-2phr	7.1 ± 0.05	413 ± 6
NR-NCW-RH-3phr	6.5 ± 0.2	422 ± 4
NR-NCW-RH-4phr	6.3 ± 0.1	430 ± 3

According to the literature, the contact angle of water for NR is higher, and cellulose is lower. Moreover, the surface morphology, like roughness on the surface, also affects the contact angle measurement. According to literature, as roughness increases, contact angle decreases [2]. The images given in Fig. 13(b) support the explanation given above.

3.16 Biodegradability studies

Biodegradable nanocomposites have wide applications in the packaging industry. Even though certain microorganisms degrade natural rubber, it is a prolonged process in natural rubber compared to the degradation of cellulose

Fig. 13 (**a**) Q_t vs. time$^{1/2}$ graph of NR-gum and NR-NCW-RH composites and (**b**) contact angle images of NR gum, NR-NCW-2phr, NR-NCW-RH-2phr

NR gum (Avg. angle ~ 99.4°)

NR-NCW-2phr (Avg. angle ~ 64.5°)

NR-NCW-RH-2phr (Avg. angle ~ 75°)
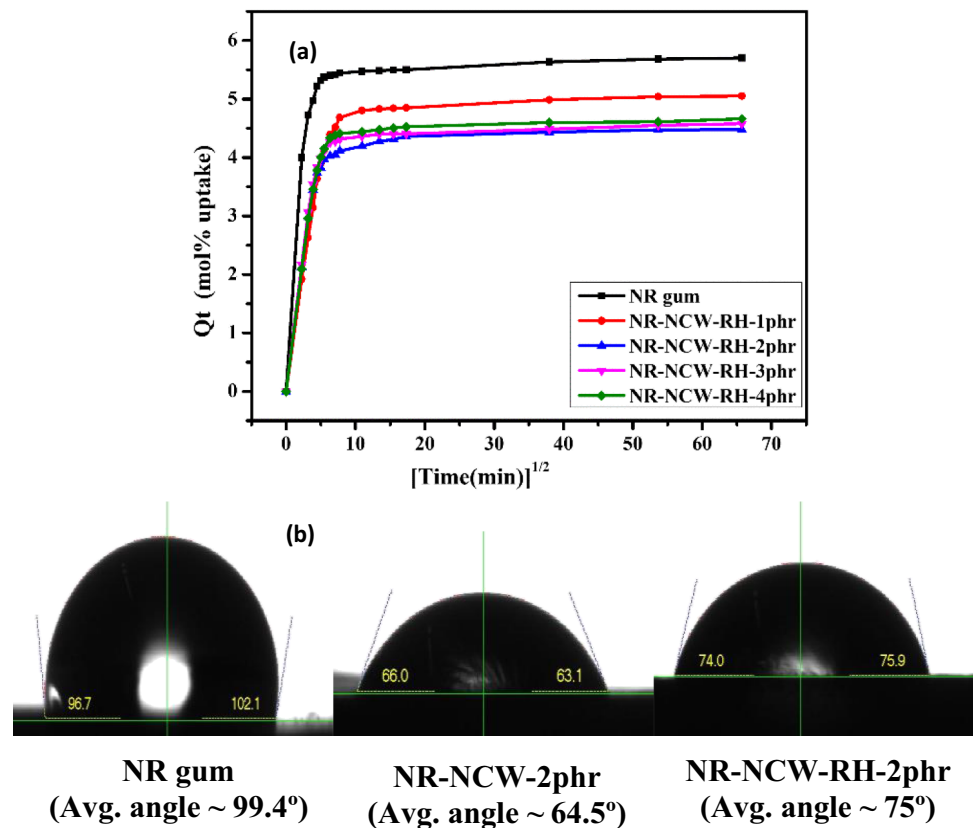
[47]. In this work, the effect of modified nanocellulose whiskers in the biodegradability of natural rubber is studied by varying the compositions of NCW. From Fig. 14(a), it is clear that the presence of NCW significantly influences the degradation of natural rubber in soil. After 9 weeks, NR gum degraded about 3.3%. But the degradation percentages of NR-NCW-RH composites are 3.9, 4.5, 4.7, and 5% respectively for 1, 2, 3, and 4phr composites. As the filler loading increases, the degradation rate also increases. As the biodegradation of cellulose is faster than rubber, the cellulose content in the composite is consumed by the microorganisms at a faster rate. It may lead to the formation of voids and porosity in the composite producing the destruction of natural rubber into small pieces. Hence, an overall faster decomposition of natural rubber is observed for NR composites containing cellulose, which agrees with the literature [48].

3.17 Permeability studies

The variation in relative permeability of original and modified samples is shown in Fig. 14(b). The shape and high aspect ratio of fillers in nano-filled latex membranes contribute to their improved gas barrier properties [49]. The modified filler has better interfacial adhesion with the rubber matrix. By reducing NCW agglomeration, the hydrogen bonding interaction between NCW and RH allows for improved dispersion. As a result, it can obstruct the flow of nitrogen gas, lowering the composite's permeability. The values of relative permeability are given in Table 9.

4 Conclusion

Elastomeric composites have wide application in the current era due to their unique properties. This study investigated the characteristic analysis of the modification done on nanocellulose whiskers to improve their properties. FTIR analysis

Table 9 Nitrogen permeability values of NR-gum, NR-NCW and NR-NCW-RH composites

Sample	Nitrogen permeability (10^{-13} cm^3 m^{-2} day^{-1})	Relative permeability (P/P_o)
NR gum	2.77	1
NR-NCW-2phr	2.74	0.9892
NR-NCW-RH-2phr	2.302	0.83104

reveals the successful incorporation of RH in NCW which is represented by their characteristic peaks in the modified sample. Morphological analysis like FESEM and HRTEM images displays the modification of NCW. EDX gives a clear idea about the absence of any other elements present in the sample also confirming the purity of NCW after modification. After modification, the average particle size obtained from DLS analysis is also in the nanometer range. A dramatic increase in the thermal stability is the most critical changes after modification of NCW with resorcinol-hexamethylene complex. In the present study, the NR-NCW-RH composites in different compositions are also prepared, and their characteristic properties are analysed. TEM analysis gave an idea about the segregated network structure formed in the composite. About 26% increase of tensile strength is observed for NR-NCW-2phr composite compared to NR gum. The enhanced interfacial interaction is confirmed by the higher storage modulus and lower tan δ value for the NR-NCW-RH-2phr composite compared to the unmodified composite. An increase in volume percentage of immobilised polymer chains (C_v) and a decrease in adhesion factor (A) also brings about an increase in the extent of interaction between NR and NCW-RH. The semicircular curves in the cole-cole plot are an indication of homogeneity in the composite. The crosslink density of the same composite about 45% higher than the NR gum implies the superior interaction between the filler and matrix. The thermal stability of the 2 phr composite increases significantly. The use of biofiller is an advantage for improving the rate of degradation of the matrix. As the concentration of the filler increases, the rate of biodegradability of the composite also increases.

Fig. 14 (**a**) Biodegradability studies of NR gum and NR-NCW-RH composites and (**b**) nitrogen permeability studies of NR gum, NR-NCW and NR-NCW-RH composites
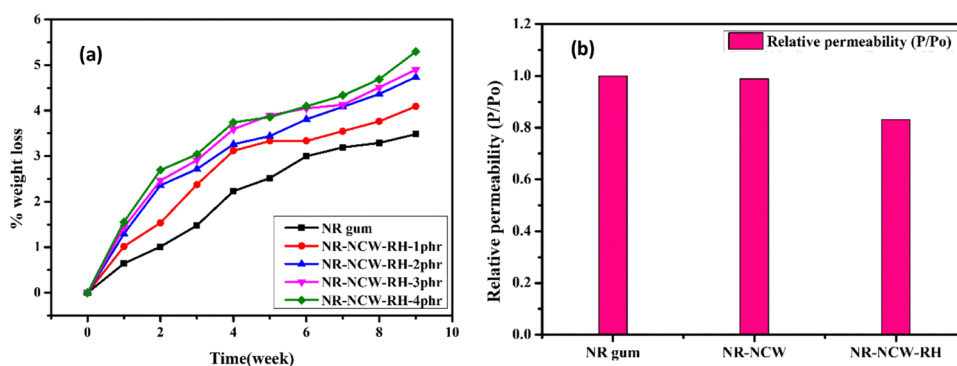
The modified filler makes the composite more impermeable to nitrogen gas compared to the unmodified one. Based on the presented results, it is possible to conclude that RH-modified NCW could be used as an effective biofiller in NR latex for high performance applications. Additionally, grafting of nanocellulose can improve its qualities even more. The current work shows how increasing the physico-mechanical properties of the composites at lower filler concentrations. The fillers can even use at higher concentrations to investigate if they have a good reinforcing effect. It is also possible to employ elastomers other than natural rubber in the composite formation and modify the surface of cellulose molecules with compounds other than resorcinol and hexamethylenetetramine to prepare polymer nanocomposites with remarkable properties.

Data availability All of the data sets that were included and/or examined in the present study can be obtained from the corresponding author upon request.

Declarations

Ethics approval This article does not contain any study with humans or animal participants.

Competing interests The authors declare no competing interests.

References

1. Rosli NA, Ahmad I, Anuar FH, Abdullah I (2019) Application of polymethylmethacrylate-grafted cellulose as reinforcement for compatibilised polylactic acid/natural rubber blends. Carbohydr Polym 213:50–58. https://doi.org/10.1016/j.carbpol.2019.02.074

2. Phomrak S (2017) Phisalaphong M (2017) Reinforcement of natural rubber with bacterial cellulose via a latex aqueous microdispersion process. J Nanomater. https://doi.org/10.1155/2017/4739793

3. Ghasemlou M, Daver F, Ivanova EP et al (2021) Surface modifications of nanocellulose: from synthesis to high-performance nanocomposites. Prog Polym Sci 119:101418. https://doi.org/10.1016/j.progpolymsci.2021.101418

4. Rafieian F, Hosseini M, Jonoobi M, Yu Q (2018) Development of hydrophobic nanocellulose-based aerogel via chemical vapor deposition for oil separation for water treatment. Cellulose 25:4695–4710. https://doi.org/10.1007/s10570-018-1867-3

5. Jiang W, Li L (2020) Surface modification of nanocrystalline cellulose and its application in natural rubber composites:1–10. https://doi.org/10.1002/app.49163

6. Yasin S, Hussain M, Zheng Q, Song Y (2021) Effects of ionic liquid on cellulosic nanofiller filled natural rubber bionanocomposites. J Colloid Interface Sci 591:409–417. https://doi.org/10.1016/j.jcis.2021.02.029

7. Xu S, Gu J, Luo Y, Jia D, Yan L (2014) Influence of nanocrystalline cellulose on structure and properties of natural rubber/silica composites. Polym Compos 16:101–113

8. Chen WJ, Gu J, Xu SH (2014) Exploring nanocrystalline cellulose as a green alternative of carbon black in natural rubber/butadiene rubber/styrene-butadiene rubber blends. Express Polym Lett 8:659–668. https://doi.org/10.3144/expresspolymlett.2014.69

9. Jiang W, Gu J (2020) Nanocrystalline cellulose isolated from different renewable sources to fabricate natural rubber composites with outstanding mechanical properties. Cellulose 27:5801–5813. https://doi.org/10.1007/s10570-020-03209-3

10. Singh S, Dhakar GL, Kapgate BP et al (2020) Synthesis and chemical modification of crystalline nanocellulose to reinforce natural rubber composites. Polym Adv Technol 31:3059–3069. https://doi.org/10.1002/pat.5030

11. Jinitha TV, Safna Hussan KP, Mohamed Shahin T, Purushothaman E (2020) The interplay between the fragility and mechanical properties of styrene–butadiene rubber composites with unmodified and modified sago seed shell powder. J Appl Polym Sci 137:1–13. https://doi.org/10.1002/app.49180

12. Jiang W, Cheng Z, Wang J, Gu J (2022) Modified nanocrystalline cellulose partially replaced carbon black to reinforce natural rubber composites. J Appl Polym Sci 139:1–9. https://doi.org/10.1002/app.52057

13. Sinclair A, Zhou X, Tangpong S et al (2019) High-performance styrene-butadiene rubber nanocomposites reinforced by surface-modified cellulose nanofibers. ACS Omega 4:13189–13199. https://doi.org/10.1021/acsomega.9b01313

14. Somseemee O, Sae-Oui P, Siriwong C (2021) Reinforcement of surface-modified cellulose nanofibrils extracted from Napier grass stem in natural rubber composites. Ind Crops Prod 171:113881. https://doi.org/10.1016/j.indcrop.2021.113881

15. Xu S, Gu J, Luo Y et al (2015) Influence of nanocrystalline cellulose on structure and properties of natural rubber/silica composites. Polym Compos 36:861–868. https://doi.org/10.1002/pc.23005

16. Seena K, Thomas PM, Sabura Begum CD, Dominic M, Salim NV, Hameed N, Mavinkere S, Siengchin SJP (2020) Isolation and characterization of cellulose nanowhiskers from Acacia caesia plant:1–9. https://doi.org/10.1002/app.50213

17. Abdel-Halim ES (2014) Chemical modification of cellulose extracted from sugarcane bagasse: Preparation of hydroxyethyl cellulose. Arab J Chem 7:362–371. https://doi.org/10.1016/j.arabjc.2013.05.006

18. Jia ZX, Luo YF, Yang SY, Guo BC, Du ML, Jia DM (2009) Morphology, interfacial interaction and properties of styrene-butadiene rubber/modified halloysite nanotube nanocomposites. Chinese J Polym Sci 27:857–864

19. Durairaj RB Resorcinol-Chemistry. In: Technology and Applications. Springer. https://doi.org/10.1007/b982897

20. Liu L, Jia D, Luo Y, Guo B (2006) Preparation, structure and properties of nitrile-butadiene rubber-organoclay nanocomposites by reactive mixing intercalation method. J Appl Polym Sci 100:1905–1913. https://doi.org/10.1002/app.22614

21. Chen W, Yu H, Liu Y et al (2011) Isolation and characterization of cellulose nanofibers from four plant cellulose fibers using a chemical-ultrasonic process. Cellulose 18:433–442. https://doi.org/10.1007/s10570-011-9497-z

22. Segal L, Creely JJ, Martin AE, Conrad CM (1959) An empirical method for estimating the degree of crystallinity of native cellulose using the x-ray diffractometer. Text Res J 29:786–794. https://doi.org/10.1177/004051755902901003

23. Dalev P, Staromanova E, Dalev D et al (2001) Biodegradation of chemically modified gelatin films in a simulated natural environment. Biotechnol Biotechnol Equip 15:116–123. https://doi.org/10.1080/13102818.2001.10819142

24. Kalita NK, Nagar MK, Mudenur C et al (2019) Biodegradation of modified Poly(lactic acid) based biocomposite films under thermophilic composting conditions. Polym Test 76:522–536. https://doi.org/10.1016/j.polymertesting.2019.02.021

25. Souza AG, Santos DF, Ferreira RR et al (2020) Innovative process for obtaining modified nanocellulose from soybean straw. Int J Biol Macromol 165:1803–1812. https://doi.org/10.1016/j.ijbiomac.2020.10.036

26. Foo ML, Tan CR, Lim PD et al (2019) Surface-modified nanocrystalline cellulose from oil palm empty fruit bunch for effective binding of curcumin. Int J Biol Macromol 138:1064–1071. https://doi.org/10.1016/j.ijbiomac.2019.07.035

27. Wang Y, Chang B, Guan D, Dong X (2015) Mesoporous activated carbon spheres derived from resorcinol-formaldehyde resin with high performance for supercapacitors. J Solid State Electrochem 19:1783–1791. https://doi.org/10.1007/s10008-015-2789-8

28. Zheng C, Chen W, Ye X (2012) Study on Au nanoparticles, TiO2 nanoclusters, and SiO 2 nanoshells coated multi-wall carbon nanotubes/silica gel-glass. Opt Mater (Amst) 34:1042–1047. https://doi.org/10.1016/j.optmat.2011.12.017

29. Hashim KKM, Manoj E, Kurup MRP (2021) A novel manganese(II) bisthiocarbohydrazone complex: crystal structures, Hirshfeld surface analysis, DFT and molecular docking study with SARS-CoV-2. J Mol Struct 1246:131125. https://doi.org/10.1016/j.molstruc.2021.131125

30. George N, Bipinbal PK, Bhadran B et al (2017) Segregated network formation of multiwalled carbon nanotubes in natural rubber through surfactant assisted latex compounding: a novel technique for multifunctional properties. Polymer (Guildf) 112:264–277. https://doi.org/10.1016/j.polymer.2017.01.082

31. Daniels ES, Klein A (1991) Development of cohesive strength in polymer films from latices: effect of polymer chain interdiffusion and crosslinking. Prog Org Coatings 19:359–378. https://doi.org/10.1016/0033-0655(91)80018-E

32. Supanakorn G, Taokaew S, Phisalaphong M (2021) Ternary composite films of natural rubber, cellulose microfiber, and carboxymethyl cellulose for excellent mechanical properties, biodegradability and chemical resistance. Cellulose 4. https://doi.org/10.1007/s10570-021-04082-4

33. Dominic CDM, Joseph R, Begum PMS et al (2020) Cellulose nanofibers isolated from the cuscuta reflexa plant as a green reinforcement of natural rubber. Polymers (Basel) 12:814. https://doi.org/10.3390/polym12040814

34. Blanchard R, Ogunsona EO, Hojabr S et al (2020) Synergistic cross-linking and reinforcing enhancement of rubber latex with cellulose nanocrystals for glove applications. ACS Appl Polym Mater 2:887–898. https://doi.org/10.1021/acsapm.9b01117

35. Agrebi F, Ghorbel N, Bresson S et al (2019) Study of nanocomposites based on cellulose nanoparticles and natural rubber latex by ATR/FTIR spectroscopy: the impact of reinforcement. Polym Compos 40:2076–2087. https://doi.org/10.1002/pc.24989

36. Idicula M, Malhotra SK, Joseph K, Thomas S (2005) Dynamic mechanical analysis of randomly oriented intimately mixed short banana/sisal hybrid fibre reinforced polyester composites. Compos Sci Technol 65:1077–1087. https://doi.org/10.1016/j.compscitech.2004.10.023

37. Joseph S, Sreekumar PA, Kenny JM, Puglia D, Thomas S, Joseph K Dynamic mechanical analysis of oil palm microfibril-reinforced acrylonitrile butadiene rubber composites. Polym Compos 16:101–113. https://doi.org/10.1002/pc.20791

38. Gheith MH, Aziz MA, Ghori W et al (2019) Flexural, thermal and dynamic mechanical properties of date palm fibres reinforced epoxy composites. J Mater Res Technol 8:853–860. https://doi.org/10.1016/j.jmrt.2018.06.013

39. Chee SS, Jawaid M, Sultan MTH et al (2019) Thermomechanical and dynamic mechanical properties of bamboo/woven kenaf mat reinforced epoxy hybrid composites. Compos Part B Eng 163:165–174. https://doi.org/10.1016/j.compositesb.2018.11.039

40. Formela K, Hejna A, Piszczyk Ł et al (2016) Processing and structure–property relationships of natural rubber/wheat bran biocomposites. Cellulose 23:3157–3175. https://doi.org/10.1007/s10570-016-1020-0

41. Abraham E, Thomas MS, John C et al (2013) Green nanocomposites of natural rubber/nanocellulose: membrane transport, rheological and thermal degradation characterisations. Ind Crops Prod 51:415–424. https://doi.org/10.1016/j.indcrop.2013.09.022

42. Bendahou A, Kaddami H, Dufresne A (2010) Investigation on the effect of cellulosic nanoparticles' morphology on the properties of natural rubber based nanocomposites. Eur Polym J 46:609–620. https://doi.org/10.1016/j.eurpolymj.2009.12.025

43. Siqueira G, Bras J, Dufresne A (2010) Cellulosic bionanocomposites: a review of preparation, properties and applications. Polymers (Basel) 2:728–765. https://doi.org/10.3390/polym2040728

44. Dileep P, Jacob S, Chandra CSJ et al (2021) Functionalized nanosilica for vulcanization efficiency and mechanical properties of natural rubber composites. Silicon 14(8):4411–4422

45. Potivara K, Phisalaphong M (2019) Development and characterization of bacterial cellulose reinforced with natural rubber. Materials (Basel) 12. https://doi.org/10.3390/ma12142323

46. Abraham J, Maria HJ, George SC et al (2015) Transport characteristics of organic solvents through carbon nanotube filled styrene butadiene rubber nanocomposites: the influence of rubber-filler interaction, the degree of reinforcement and morphology. Phys Chem Chem Phys 17:11217–11228. https://doi.org/10.1039/c5cp00719d

47. Bras J, Hassan ML, Bruzesse C et al (2010) Mechanical, barrier, and biodegradability properties of bagasse cellulose whiskers reinforced natural rubber nanocomposites. Ind Crops Prod 32:627–633. https://doi.org/10.1016/j.indcrop.2010.07.018

48. Stelescu MD, Manaila E, Craciun G, Chirila C (2017) Development and characterization of polymer eco-composites based on natural rubber reinforced with natural fibers. Materials (Basel) 10:1–20. https://doi.org/10.3390/ma10070787

49. Stephen R, Ranganathaiah C, Varghese S et al (2006) Gas transport through nano and micro composites of natural rubber (NR) and their blends with carboxylated styrene butadiene rubber (XSBR) latex membranes. Polymer (Guildf) 47:858–870. https://doi.org/10.1016/j.polymer.2005.12.020